



**Preliminary Analysis of Aluminum  $K_{\alpha}$  Satellite  
Spectra Obtained in KALIF Applied-B Diode  
Experiments**

**J.J. MacFarlane and P. Wang**

**July 1996**

**UWFDM-1028**

***FUSION TECHNOLOGY INSTITUTE  
UNIVERSITY OF WISCONSIN  
MADISON WISCONSIN***

**Preliminary Analysis of Aluminum  $K_{\alpha}$   
Satellite Spectra Obtained in KALIF Applied-B  
Diode Experiments**

J.J. MacFarlane and P. Wang

Fusion Technology Institute  
University of Wisconsin  
1500 Engineering Drive  
Madison, WI 53706

<http://fti.neep.wisc.edu>

July 1996

UWFDM-1028

**Preliminary Analysis of Aluminum  
K<sub>α</sub> Satellite Spectra Obtained in  
KALIF Applied-B Diode Experiments**

J. J. MacFarlane and P. Wang

Fusion Technology Institute  
University of Wisconsin-Madison  
1500 Engineering Drive  
Madison, WI 53706

July 1996

UWFDM-1028

## Contents

1. Introduction	1
2. Adopted Time-Dependent and Space-Dependent Beam Parameters	1
3. Numerical Procedure	5
4. Radiation-Hydrodynamics Results	7
5. Calculations of $K_\alpha$ Emission Spectra	15

## 1. Introduction

The purpose of this report is to describe recent efforts in modeling KALIF beam-plasma interaction experiments. Specifically, we report on preliminary simulations of KALIF applied-B diode experiments in which  $K_\alpha$  emission spectra from Al targets were recorded. Figure 1 shows x-ray crystal emission spectra from several KALIF shots [1]. The top plots show time- and space-integrated spectra for 2  $\mu\text{m}$ -thick (left) and 6  $\mu\text{m}$ -thick (right) Al targets. The bottom plot compares spectra obtained in  $B_\theta$  diode and applied-B diode experiments. As noted in Ref. [1], the  $K_\alpha$  spectra from the 2  $\mu\text{m}$ -thick and 6  $\mu\text{m}$ -thick target experiments are very similar, but the absolute flux deduced from the 6  $\mu\text{m}$  target appears to be roughly a factor of 2 greater. The lower plot shows that  $K_\alpha$  satellites from higher ionization stages were observable in the applied-B diode experiments ( $h\nu \approx 1.51$  keV and 1.525 keV), indicating higher temperatures were attained.

Here, we report on preliminary simulations to analyze these spectra. We do *not* present results which explain all aspects of the observed spectra. Rather, our objective is: (1) to describe several aspects of our analysis procedure (particularly in regards to the time- and space-dependent beam properties and implications for the observed  $K_\alpha$  spectra); and (2) to begin to address the sensitivity of the predicted time- and space-integrated  $K_\alpha$  spectra to the target thickness and to uncertainties in the beam parameters.

## 2. Adopted Time-Dependent and Space-Dependent Beam Parameters

Since the spectrometer views the entire area of the target which is irradiated by the beam, it will record emission from the hot “central” part of the beam as well as emission from the cooler regions away from beam center. Thus, target temperatures will depend on both the depth (perpendicular to the target surface) and the position on the target plane.

The spatial dependence of the beam is modeled using a Gaussian beam profile (see Figure 2). By dividing the target plane into several discrete regions, we can account for the space-integration effects of the spectrometer by performing a series of 1-D radiation-hydrodynamics calculations using different beam current densities for each region.

Assuming a Gaussian beam profile, a current density distribution function can be written as:

$$f(r) = \frac{1}{\pi R_0^2} e^{-(r/R_0)^2}, \quad (1)$$

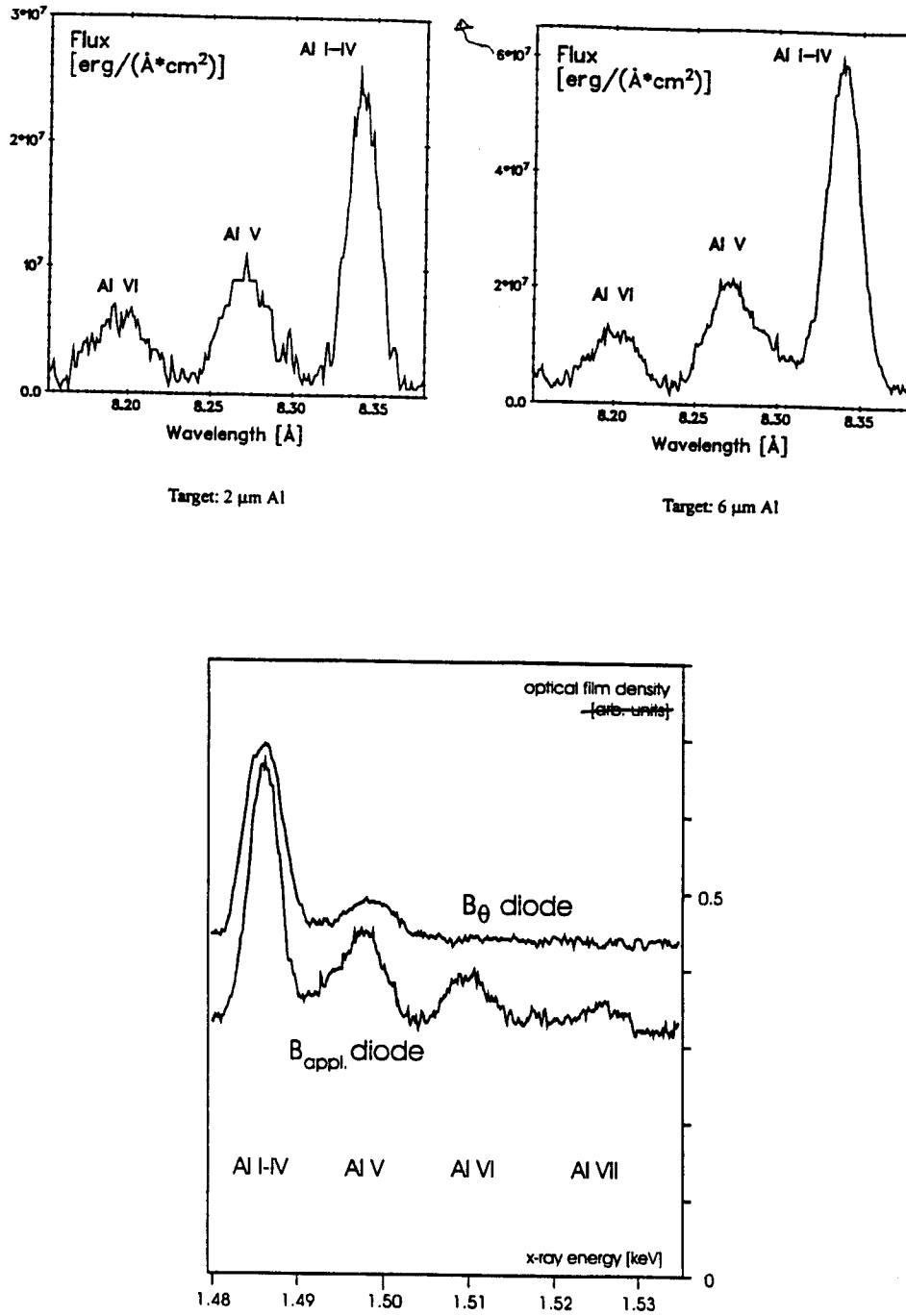
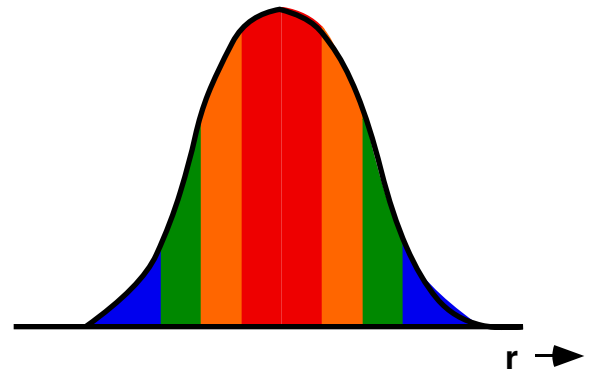
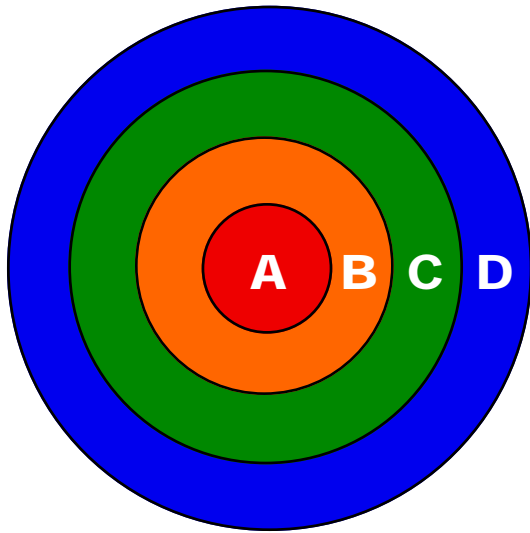


Figure 1. (Top) Comparison of  $K_\alpha$  emission spectra from 2  $\mu\text{m}$  and 6  $\mu\text{m}$  Al targets obtained in KALIF applied-B diode experiments. (Bottom) Comparison of  $K_\alpha$  emission spectra from KALIF  $B_\theta$  diode and applied-B diode shots (from Ref. [1]).



**Gaussian beam profile**

Figure 2. Schematic illustration of assumed Gaussian current density distribution on the target plane.

where  $r$  is distance from the center of the beam (which is assumed to be cylindrically symmetric), and  $R_0$  is a constant which is related to a measured beam diameter by:

$$R_0 = \frac{\text{FWHM}}{2(\ln 2)^{1/2}}, \quad (2)$$

where FWHM is the full width (diameter) of the beam at half maximum.

The current contained in a region between  $r_1$  and  $r_2$  is then given by:

$$\begin{aligned} I(r_1, r_2) &= 2\pi I_{\text{TOT}} \int_{r_1}^{r_2} dr r f(r) \\ &= I_{\text{TOT}} [e^{-(r_1/R_0)^2} - e^{-(r_2/R_0)^2}], \end{aligned} \quad (3)$$

where  $I_{\text{TOT}}$  is the total current ( $0 < r < \infty$ ).

The mean current density in a region between  $r_1$  and  $r_2$  can be written as:

$$J(r_1, r_2) = \frac{I(r_1, r_2)}{\pi(r_2^2 - r_1^2)}. \quad (4)$$

Note that at the center of the beam ( $r \rightarrow 0$ ), the peak current density is:

$$J_{\text{peak}} = \frac{I_{\text{TOT}}}{\pi R_0^2}. \quad (5)$$

In the simulations described below, the beam profile has been divided into 4 regions on the target plane. The outer radius, current, current density, and area ( $A$ ) of each region is given in Table 1.

**Table 1. Region-Dependent Beam Conditions on Target Plane**

Region	$r/R_0$	$I/I_{\text{tot}}$	$A/\pi R_0^2$	$J/J_{\text{peak}}$
A	0.5	0.221	0.250	0.884
B	0.8	0.252	0.390	0.646
C	1.2	0.290	0.800	0.363
D	2.0	0.219	2.56	0.086

Note that the total current in the 4 regions is  $0.982 I_{\text{tot}}$ . Thus, less than 2% of the current resides outside  $2R_0$  in this model.

Radiation-hydrodynamics simulations are performed for each region using the current density multipliers in Table 1. The time-dependence of the beam enters through

$J_{\text{peak}}(t)$ . Thus,  $J_{\text{peak}}$  and  $I_{\text{tot}}$  vary in time, while all other quantities in Table 1 are assumed to be time-independent. (This of course assumes the beam does not move in the target plane and has a constant “radius”  $R_0$ .) The time-dependence of the peak beam current density is taken from experimental beam diagnostics [2], and is shown in Figure 3 along with the proton beam voltage. This is identical to the time-dependent beam current density used in shock wave physics simulations reported in Ref. [3]. The peak power density corresponding to the curves shown in Figure 3 is  $P_B(\text{max}) = 0.84 \text{ TW/cm}^2$ . At this time, the current density and voltage are  $0.50 \text{ MA/cm}^2$  and  $1.69 \text{ MeV}$ , respectively.

Note that the current density used in the radiation-hydrodynamics simulations of the central region (Region A) is given by:

$$J(\text{Region A}) = 0.884 J_{\text{peak}}(t). \quad (6)$$

That is, it is 12% less than the “peak current density” inferred from the beam diagnostics. It is also worth noting that the “mean” current density contained within a radius of  $\text{FWHM}/2 (= 0.833 R_0)$  is:

$$\begin{aligned} J(0 < r < 0.5 \text{ FWHM}) &= J_{\text{peak}} \cdot \frac{1 - e^{-(0.833)^2}}{(0.833)^2} \\ &= 0.72 J_{\text{peak}}. \end{aligned} \quad (7)$$

That is, the mean current density within a spot defined by the FWHM diameter is only 72% of the peak value of the Gaussian distribution. These factors should be considered in checking the consistency between the beam parameters used in the simulations versus those deduced from the beam diagnostic measurements.

### 3. Numerical Procedure

For each of the 4 regions, 1-D radiation-hydrodynamics calculations are performed using BUCKY-1 [4] to get the space- (i.e., depth-) and time-dependent temperature, density, beam voltage, and ion flux (beam current density) in the target. The results at 10 ns intervals are output to a file which can be read by our CRE code NLTERT [5], which utilizes cross sections calculated using ATBASE [6]. For each of the hydro simulation outputs (10 ns, 20 ns, ... , 70 ns) CRE calculations are performed to compute the emergent  $K_\alpha$  satellite spectrum from the rear side of the Al target (opposite to the side where the proton beam enters). This is done for each of the four regions. Each region’s spectra are then post-processed to produce a time-integrated spectrum which includes instrumental broadening (with  $\lambda/\Delta\lambda = 1000$  [1]). The four time-integrated spectra are then spatially integrated using the areal weights given in Table 1.

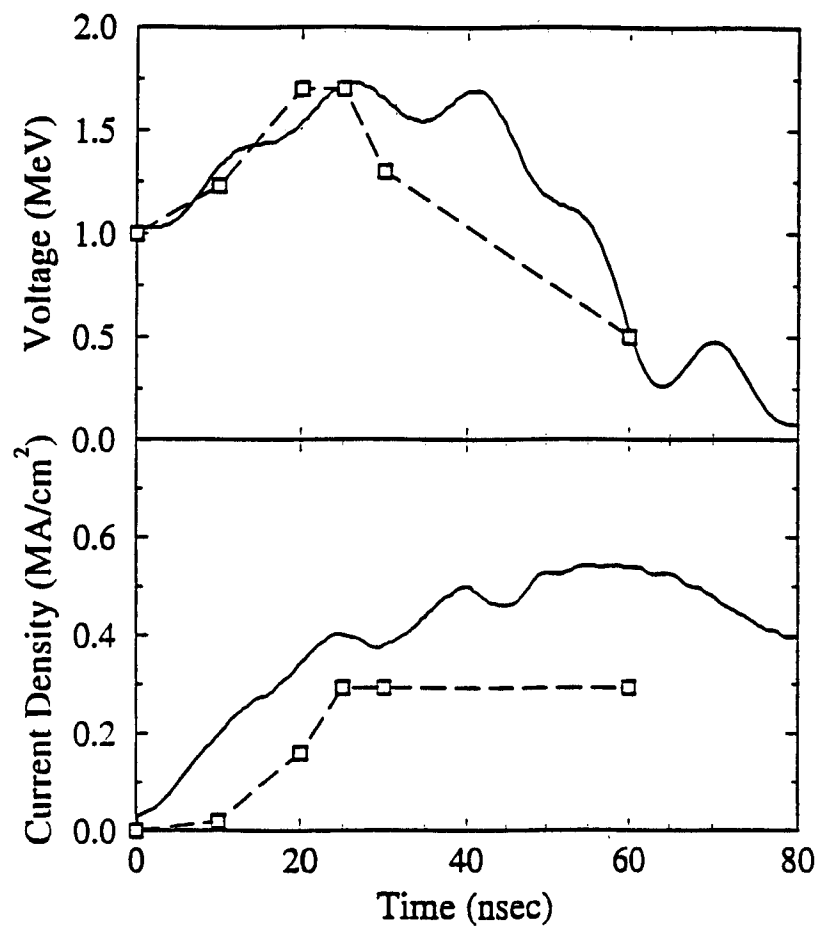


Figure 3. Time-dependent proton beam voltage and peak current density used in radiation-hydrodynamics simulations. (solid curves).

## 4. Radiation-Hydrodynamics Results

Four series of calculations have been performed. The baseline case is for a 6  $\mu\text{m}$ -thick Al target with the “nominal” beam parameters described above. A second series of calculations was performed for a 2  $\mu\text{m}$ -thick Al target with the nominal beam parameters. In the third and fourth series of calculations, a 6  $\mu\text{m}$ -thick Al target was irradiated using a more intense beam ( $J(t) = 1.25$  times the nominal beam) and a less intense beam ( $J(t) = 0.75$  times nominal).

Results from the baseline 6  $\mu\text{m}$  case are shown in Figures 4 through 10. Figure 4 shows the mean temperature in the Al as a function of time for each of the 4 spatial regions. The mean temperature is given by:

$$\langle T \rangle = \frac{\sum_j m_j T_j}{\sum_j m_j}, \quad (8)$$

where  $m_j$  and  $T_j$  are the mass (per unit area) and temperature of zone  $j$ . The temperature for the central region of the beam is seen to increase with time until it reaches a maximum of just over 30 eV. The other spatial regions are lower, with the temperature in the outermost region (Region D) remaining below 10 eV throughout the beam pulse.

Figures 5 through 8 show, for the central region of the beam, the temperature, density, specific internal energy, and time-integrated specific ion beam energy deposited as a function of position in the target. In these plots, the beam enters at the left ( $m = 0$ ). Results are shown for simulation times at 10 ns intervals up to 80 ns. Figure 5 shows the temperature is roughly uniform and steadily increases with time up to about 60 ns. At that time, the temperature is slightly over 30 eV. At later times, due to both the drop-off in the beam voltage and range shortening, the beam ranges out in the target and only the front side of the target continues to be heated.

Interestingly, the peak temperature on the front side of the target rises from roughly 30 eV at 60 ns, to over 60 eV at 80 ns. The reason this occurs is as follows. During this time, about 2.5 kJ/cm<sup>2</sup> (or about 8% of the 30 kJ/cm<sup>2</sup> beam ion energy in this simulation of the central region) is deposited to a depth of  $\sim 2 \times 10^{-4}$  g/cm<sup>2</sup>. This leads to an increase in the internal energy of the plasma of  $\sim 10^7$  J/g, as shown in Figures 7 and 8.

It is also worth noting that the beam power density during this time is 0.1 to 0.2 TW/cm<sup>2</sup>. By comparison the flux radiated from the front side surface (shown in Figure 9) is less than 0.1 TW/cm<sup>2</sup>. The radiative flux from the front side surface can be significantly lower than the blackbody flux corresponding to the surface temperature

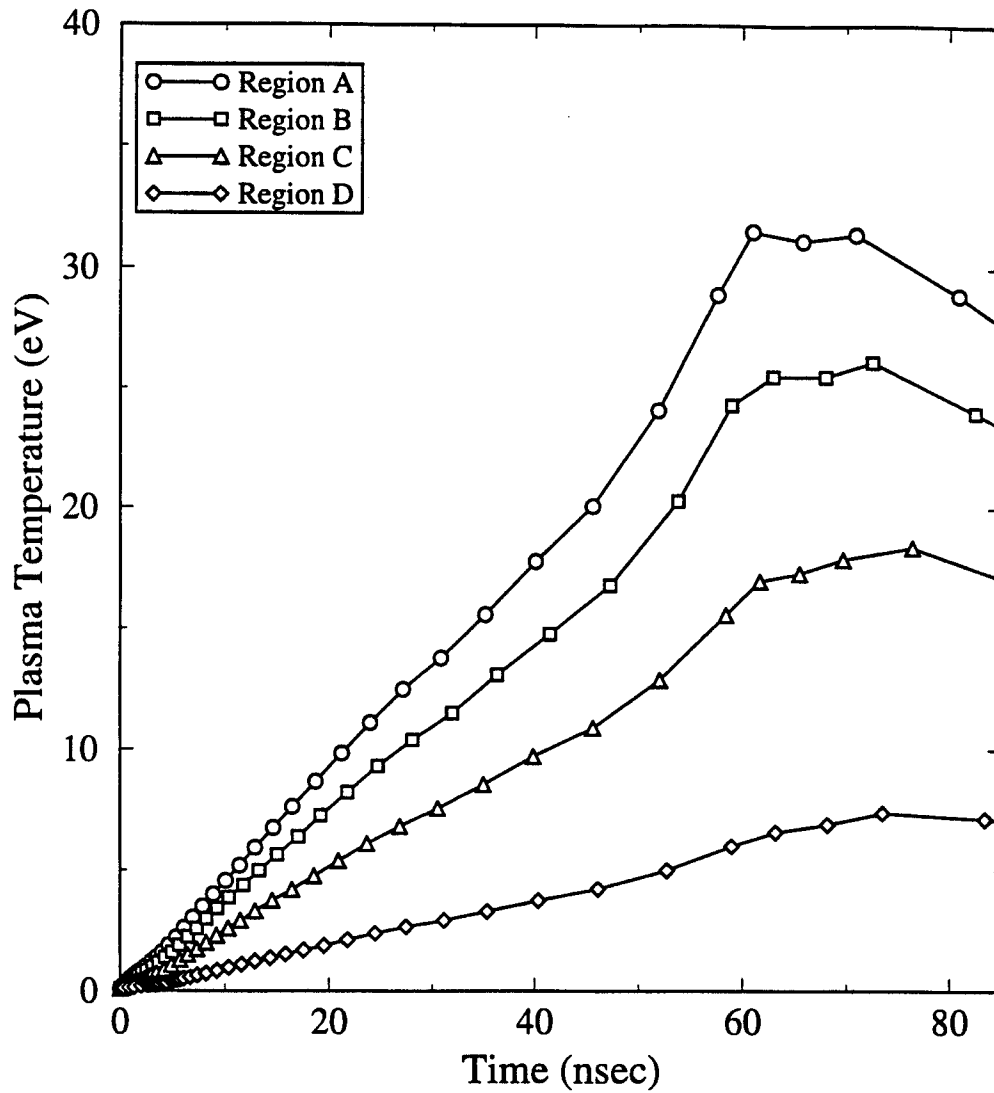


Figure 4. Time dependence of mean temperature in the Al target. Regions A through D represent different areas of the target plane (see Figure 2).

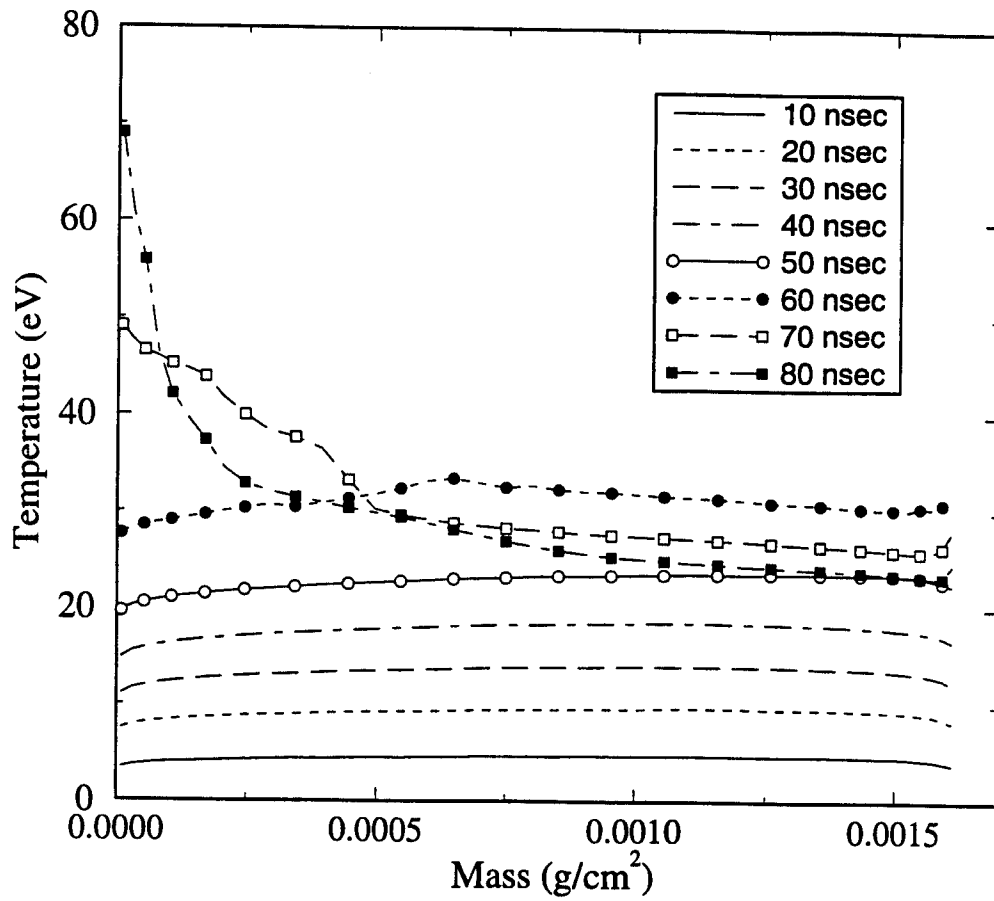


Figure 5. Temperature distribution in 6  $\mu\text{m}$  Al target at several rad-hydro simulation times (for Region A, nominal beam case).

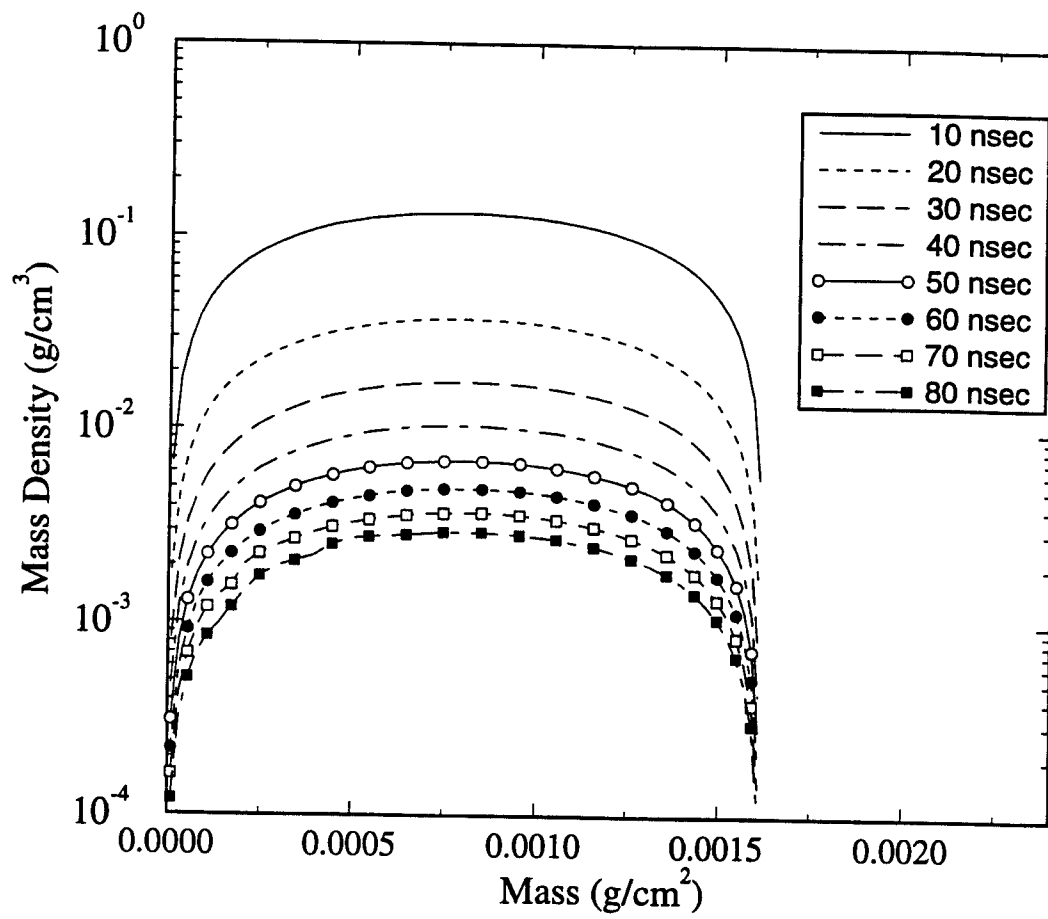


Figure 6. Mass density distributions for same simulation as in Figure 5.

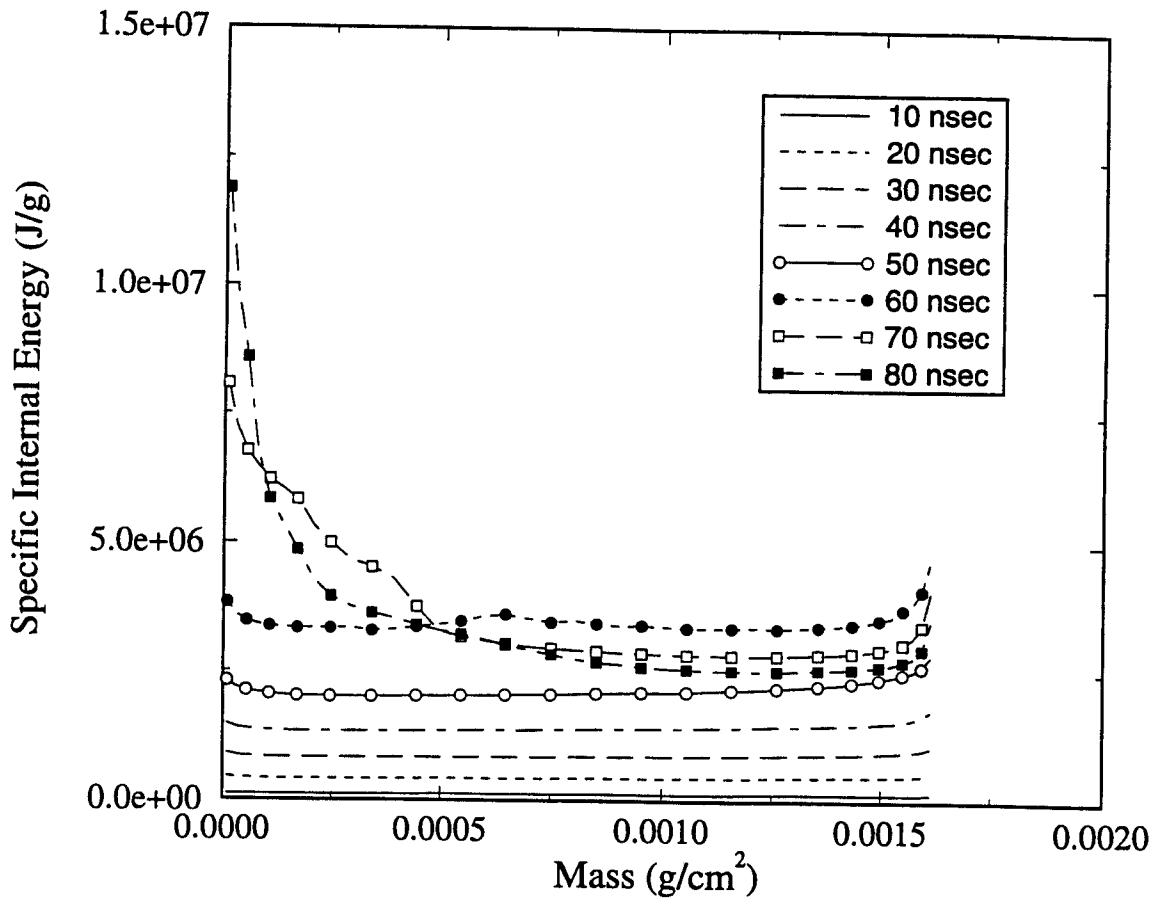


Figure 7. Specific internal energy distributions for same simulation as in Figure 5.

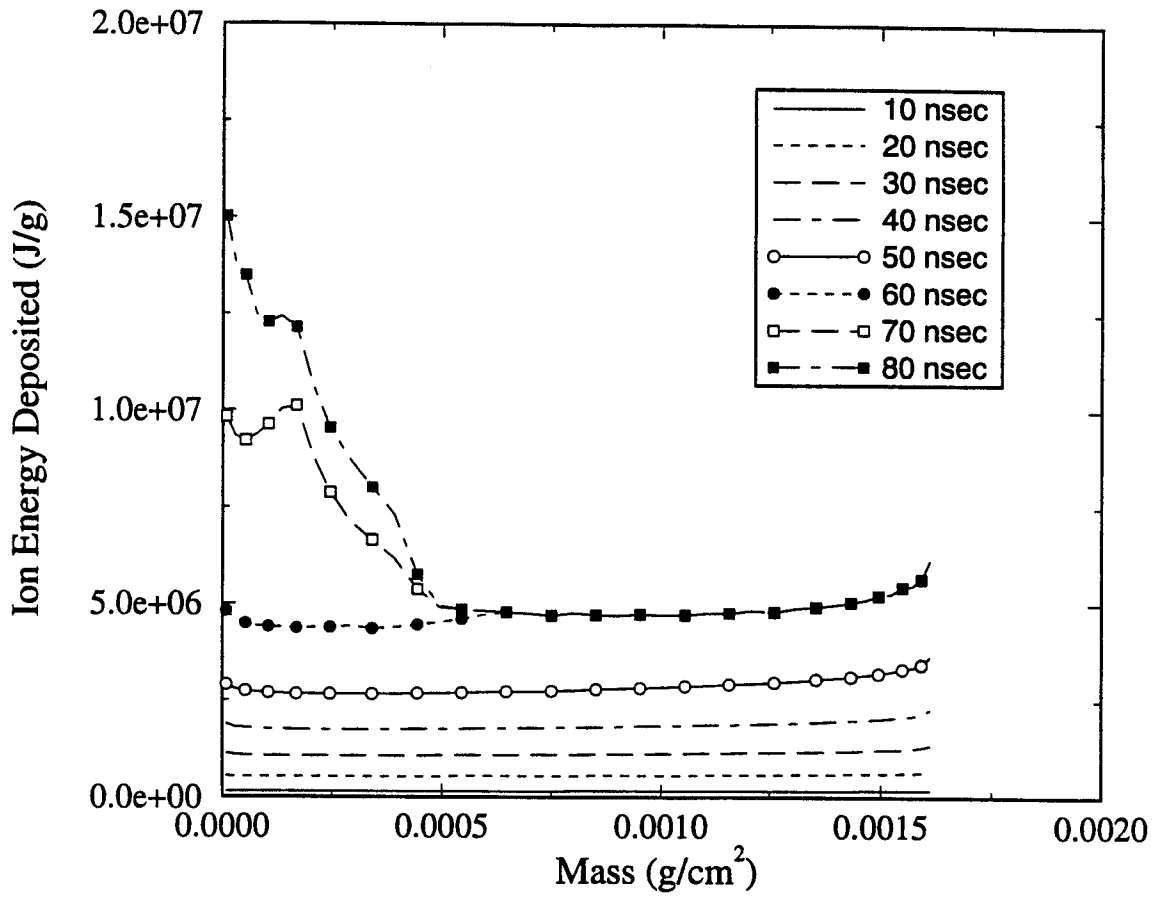


Figure 8. Time-integrated proton beam energy deposition distributions for same simulation as in Figure 5.

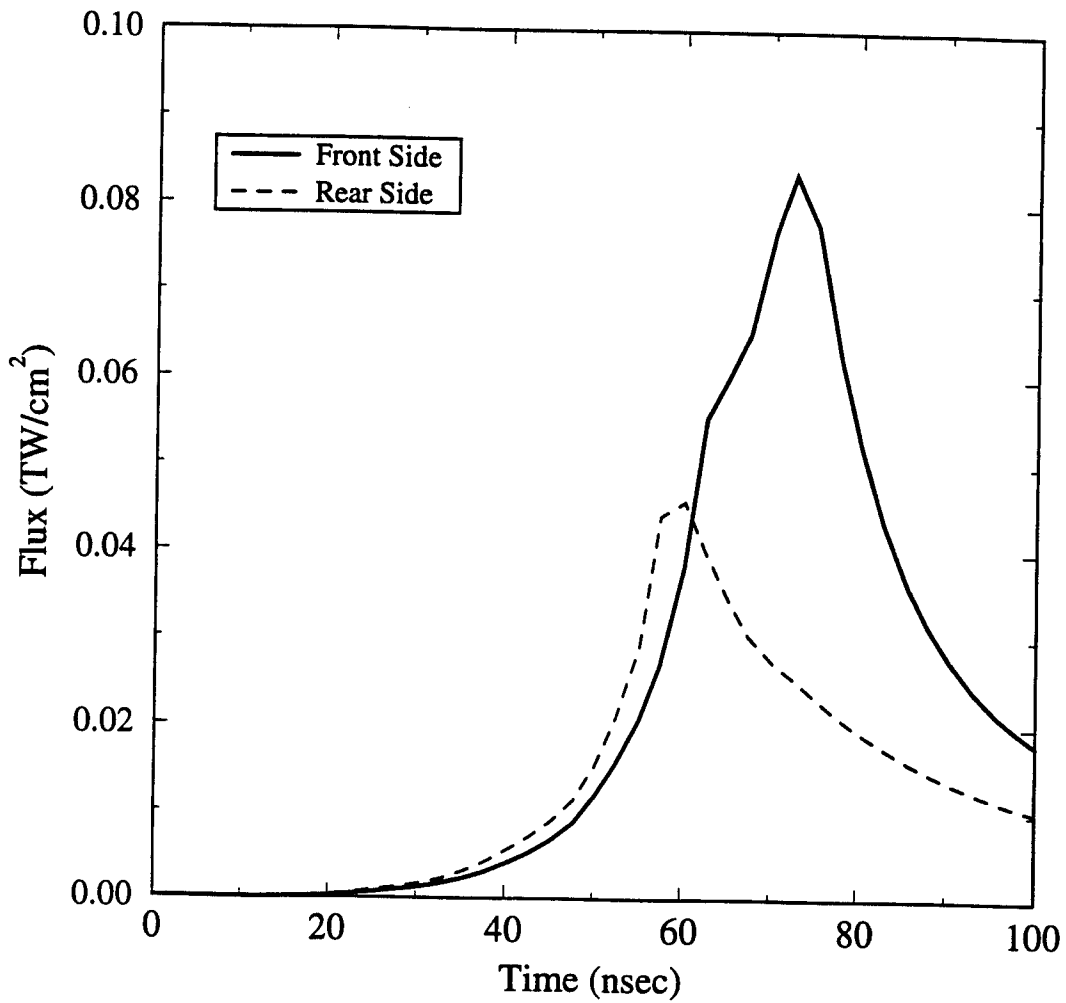


Figure 9. Time-dependence of radiation flux emitted from front (beam-irradiated) and rear sides of target for 6  $\mu\text{m}$  Al baseline simulation.

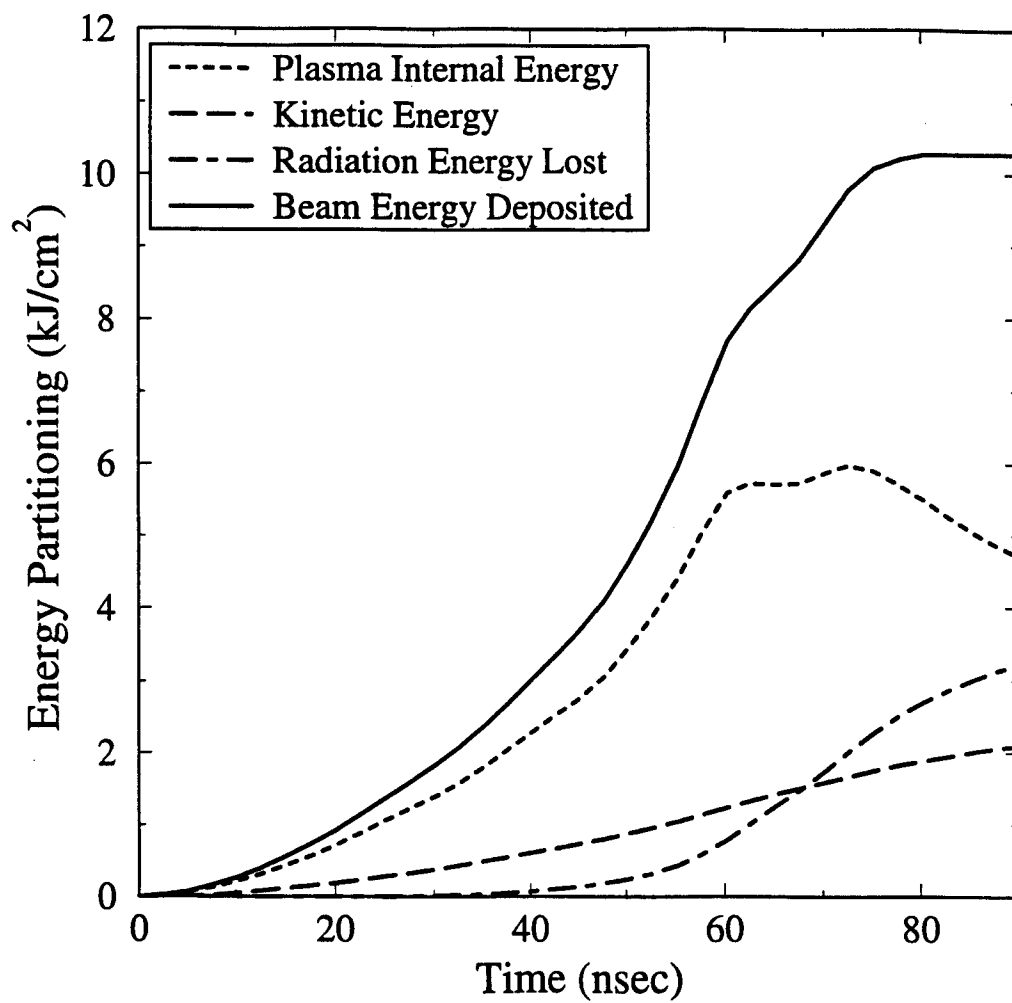


Figure 10. Energy partitioning in 6  $\mu\text{m}$  Al baseline simulation (Region A).

because the continuum optical depth of the hot region is less than unity throughout much of the spectrum. Stated another way, at late times the range of the protons is significantly less than a Rosseland (opacity) mean free path.

Figure 10 shows the energy partitioning in the target as a function of time for the beam center case. The total ion beam energy deposited in the target was about  $10 \text{ kJ/cm}^2$ , or roughly one-third of the total energy of the beam. It is also seen that radiation losses are fairly insignificant during the first 40 ns of the beam pulse, which is when most of the  $K_\alpha$  photons are emitted.

The effect of the target thickness on the mean target temperature is shown in Figure 11, where the results for the  $6 \mu\text{m}$  and  $2 \mu\text{m}$ -thick (dotted curves) Al simulations are compared. The temperatures in the  $2 \mu\text{m}$  case are somewhat lower during the first 60 ns. This evidently is due to the thicker target maintaining higher mean density during its expansion. This can have a twofold effect: less expansive cooling and a lower ionization state (which leads to a higher temperature for a given specific internal energy). At later times the  $2 \mu\text{m}$  target attains a somewhat higher *mean* temperature. This is simply due to the fact that the proton beam ranges out in the thicker target sooner, leading to a larger region near the rear surface which is not heated by the beam at late times.

Results from  $6 \mu\text{m}$ -thick Al simulations with an enhanced (1.25 multiplier) and reduced (0.75 multiplier) beam are shown in Figure 12. In the enhanced beam case (solid curves), the peak temperature is 36 eV, versus 26 eV for the reduced beam case. The ramifications of the enhanced or reduced temperature on the  $K_\alpha$  spectra are discussed in the next section.

## 5. Calculations of $K_\alpha$ Emission Spectra

Results for time-dependent emission spectra for the central beam region of the Al baseline series ( $6 \mu\text{m}$  Al, nominal beam) are shown in Figure 13. These results do not include instrumental broadening. At the earliest time (10 ns) the spectrum is dominated by the cold  $K_\alpha$  feature near  $\lambda = 8.33 \text{ \AA}$ . As the plasma heats up, the emission shifts to higher ionization stages. Note the change in scale for the different simulation times. At times  $\geq 50 \text{ ns}$  the emission is very weak due to the drop in the beam voltage, which leads to a lower proton-impact ionization cross section [7].

The time-integrated spectrum for the central beam region of the Al baseline case is shown by the thick solid curve in Figure 14. (Note that all time-integrated spectra include an instrumental broadening of  $\lambda/\Delta\lambda = 1000$ .) For the central beam region (Region A),

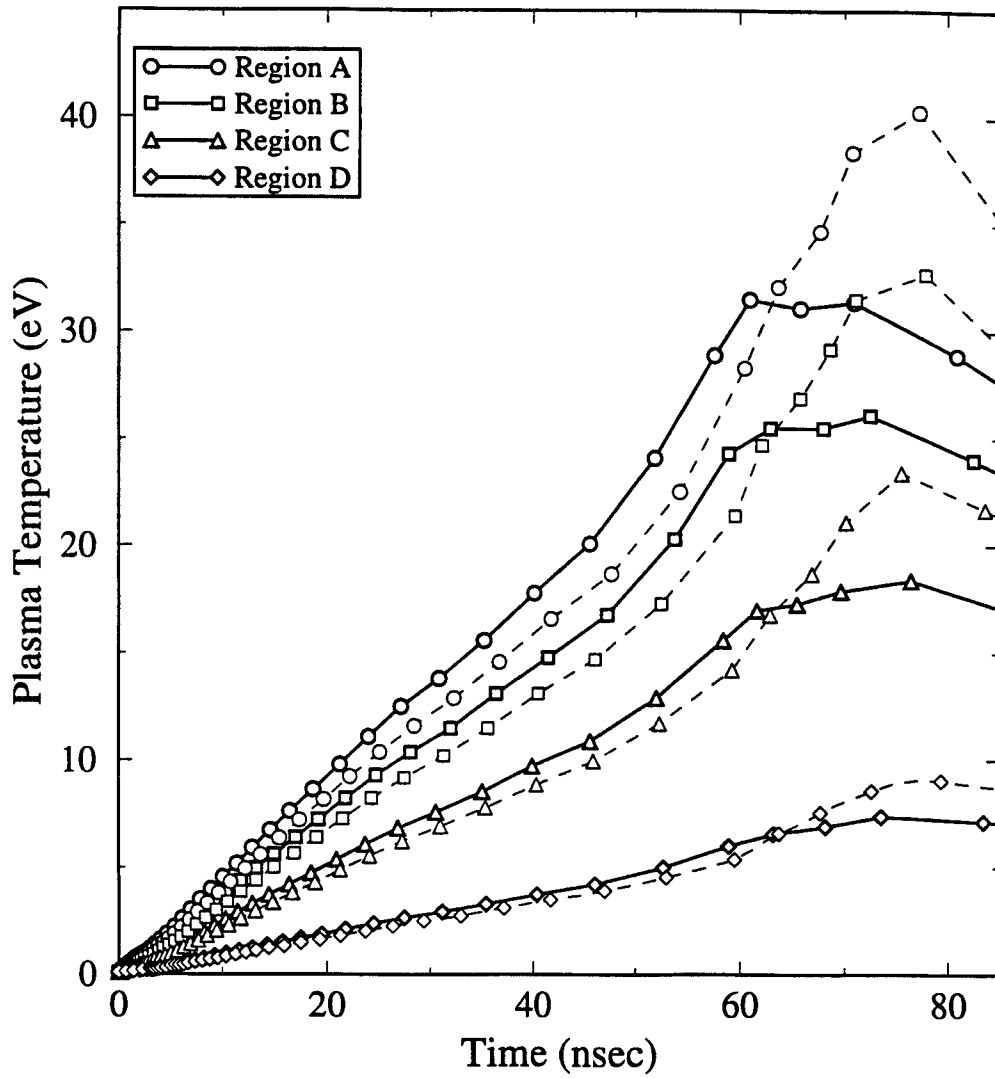


Figure 11. Comparison of mean temperatures in 2  $\mu\text{m}$  Al (dotted curves) and 6  $\mu\text{m}$  Al (solid curves) simulations.

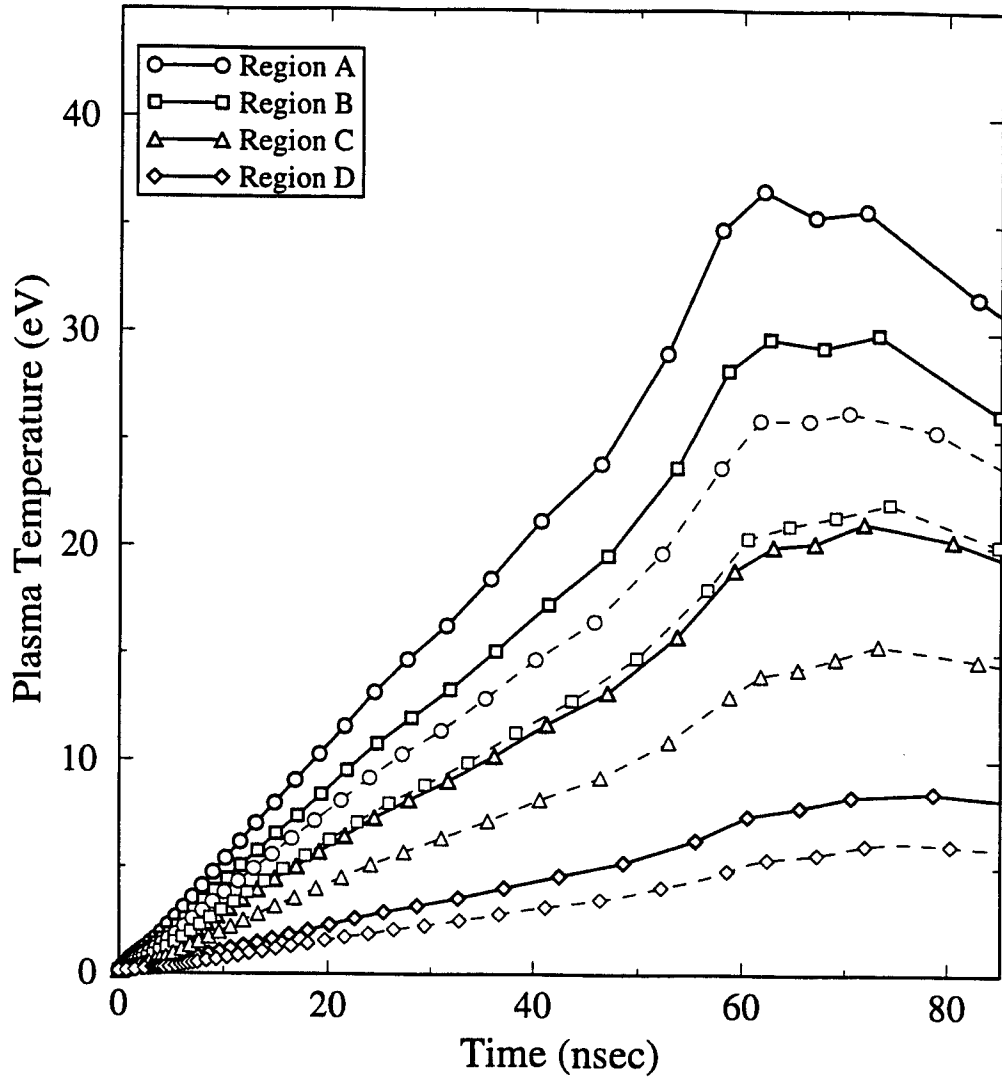


Figure 12. Evolution of mean temperatures in simulations using enhanced (multiplier = 1.25) and reduced (multiplier = 0.75) proton beam current densities.

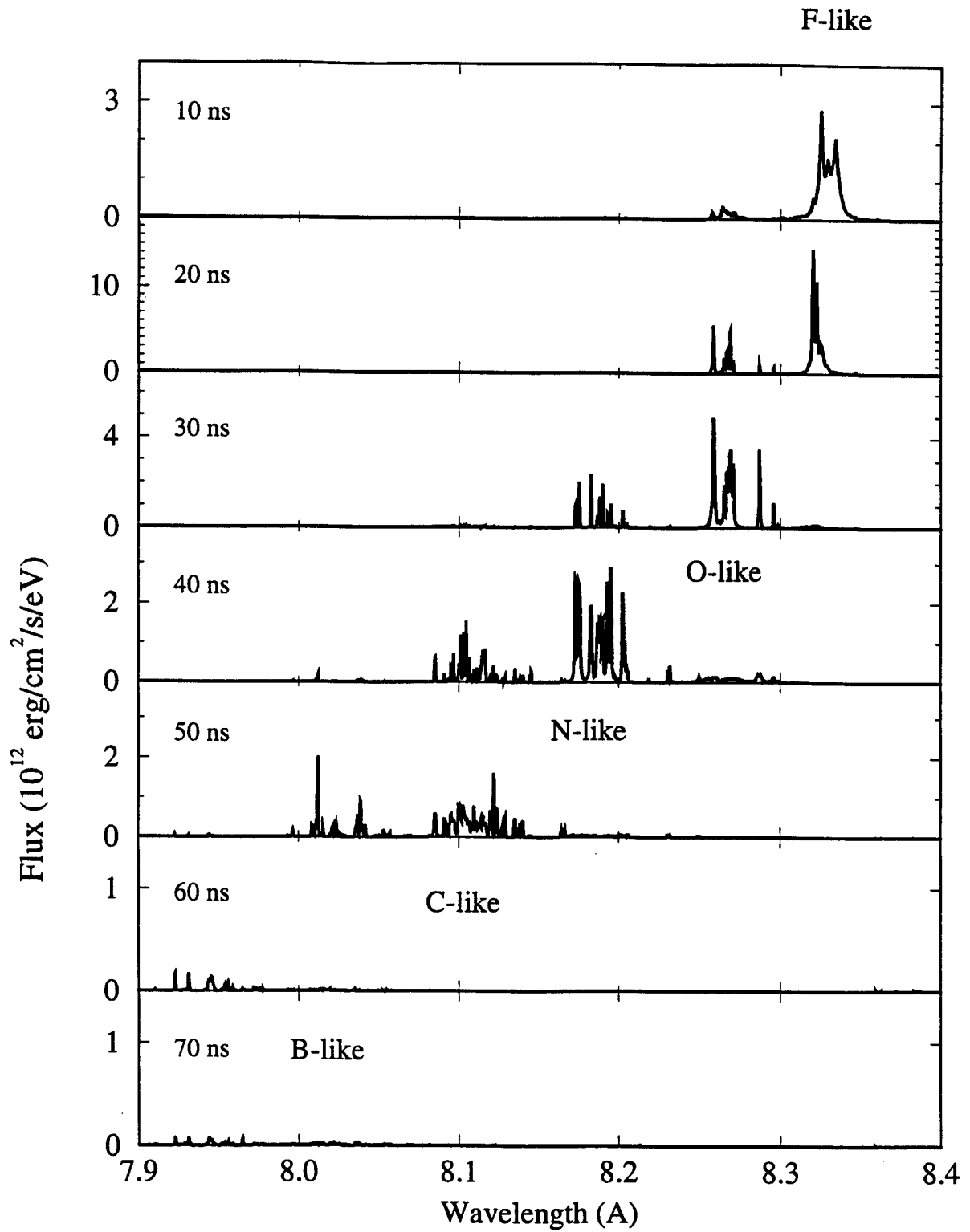


Figure 13. Time-dependent  $K_{\alpha}$  emission spectra for Region A of 6  $\mu\text{m}$  Al baseline simulation.

emission from the F-like (cold) feature is strongest, with emission from the O-, N-, and C-like features being successively weaker. For comparison, emission from the other regions in the target plan are also shown in Figure 14. For the outermost region (Region D;  $1.2 < r/R_0 < 2.0$ ) emission is by far strongest from the F-like feature, the O-like emission peak is about a factor of 8 lower, and emission from higher ionization stages is extremely weak.

Spatially integrating the results from these 4 regions leads to the space- and time-integrated spectrum shown in Figure 15 (solid curve). This result can be compared with the experimental space- and time-integrated spectrum in Figure 1 (upper right plot). Note that the ratio of the peak F-like to O-like intensities are in good agreement; both are approximately 3 in both plots. The O-like feature is more broadened in the experimental spectrum (vs. calculation). This could very well be done to F-like ions which have M-shell spectator electrons (Figure 7 of Ref. [8]), such as transitions of the type:

$$1s^2 2s^2 2p^5 3\ell \frac{\text{p-impact}}{>} > 1s^1 2s^2 2p^5 3\ell \frac{\text{K}\alpha}{>} > 1s^2 2s^2 2p^4 3\ell .$$

These types of transitions become more important for thicker targets because opacity effects tend to limit the emission from states without M-shell spectators (which are lower energy levels). In the series of calculations presented here, only a few states with M-shell spectators were included.

Figure 15 also shows that the emission from N-like feature ( $\lambda \approx 8.2 \text{ \AA}$ ) is somewhat weaker in the calculations than in the experiments. This suggests that the temperatures in the simulation may have been too low. Lower temperatures could arise from using beam current densities that are too low. Alternatively, one could hypothesize that the beam voltage in the simulation was too high at early times ( $t \lesssim 30 \text{ ns}$ ). If the beam voltage were lower, the stopping power ( $dE/dx$ ) would be higher, leading to a higher temperature. In addition, a lower beam voltage at early times would give lower proton-impact ionization cross sections, which in turn could lead to lower emission from the F-like and O-like peaks.

The sensitivity of the space- and time-integrated spectra to the beam current density is shown in Figure 16. The “enhanced” and “reduced” beams correspond to using multipliers of 1.25 and 0.75 on the nominal beam current density. Even with an enhancement of 1.25, the emission from the N-like feature is considerably lower than the O-like feature. Using an even higher beam enhancement multiplier should produce better agreement with the measured spectrum. Also, because the emission from the higher ionization features comes from the central regions of the beam (Regions A and

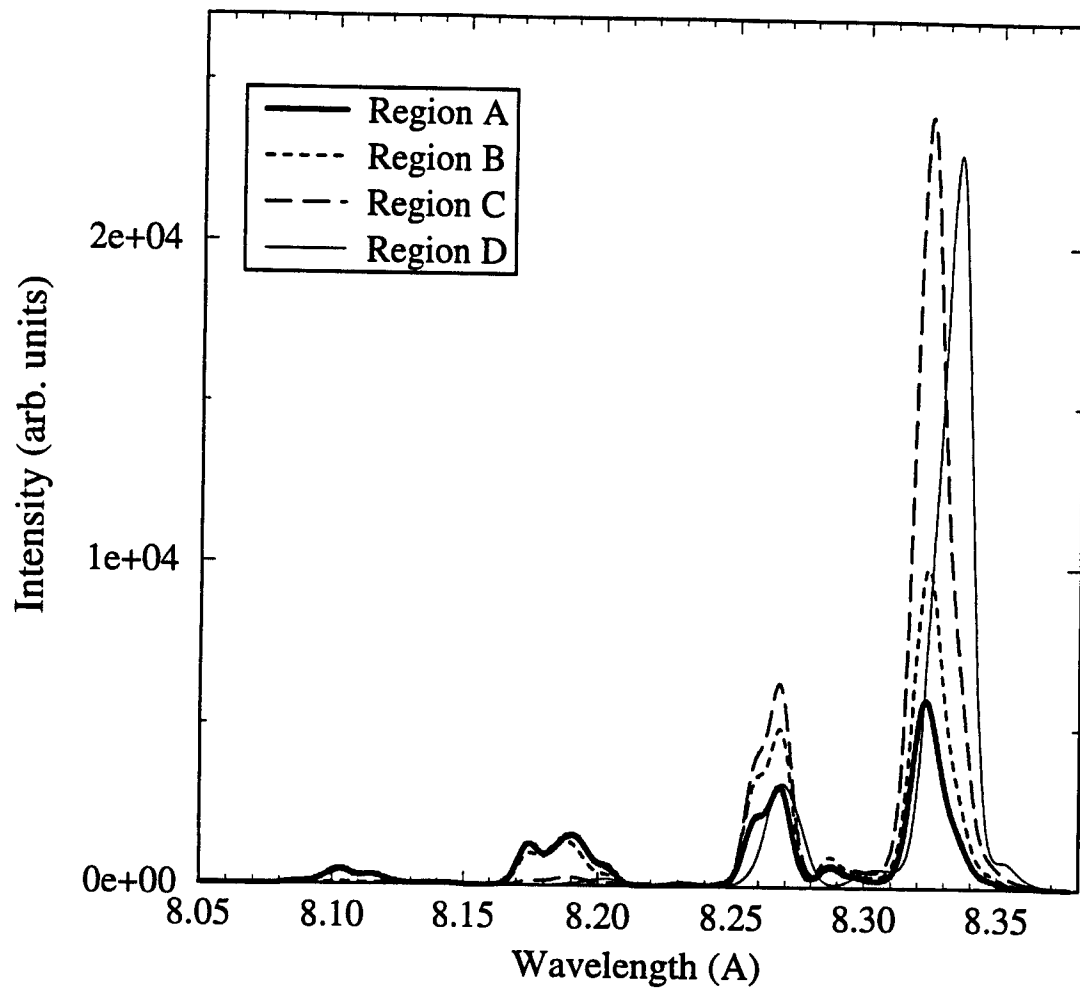


Figure 14. Area-weighted time-integrated spectra from Regions A through D for 6  $\mu\text{m}$  Al baseline simulation.

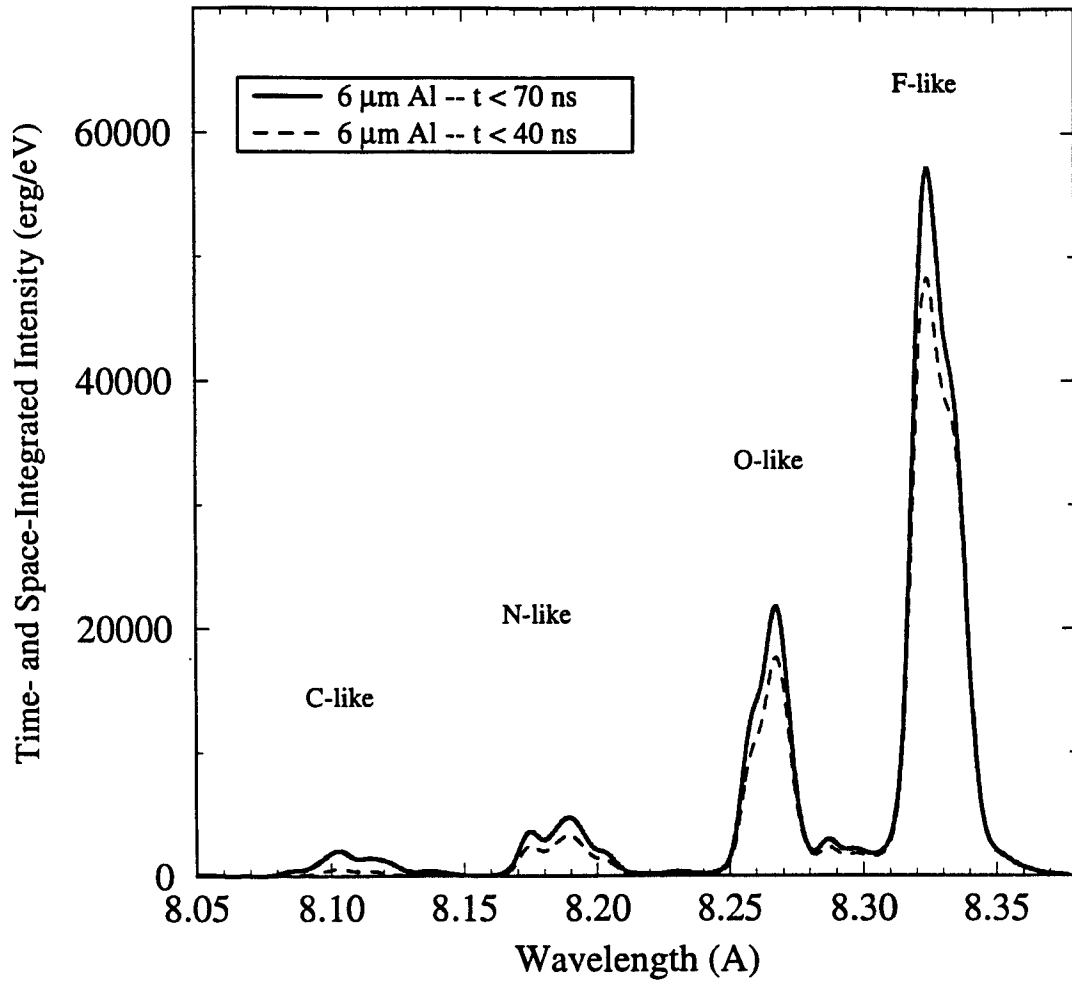


Figure 15. Space- and time-integrated (up to 40 and 70 ns)  $K_{\alpha}$  emission spectra for 6  $\mu\text{m}$  Al baseline simulation.

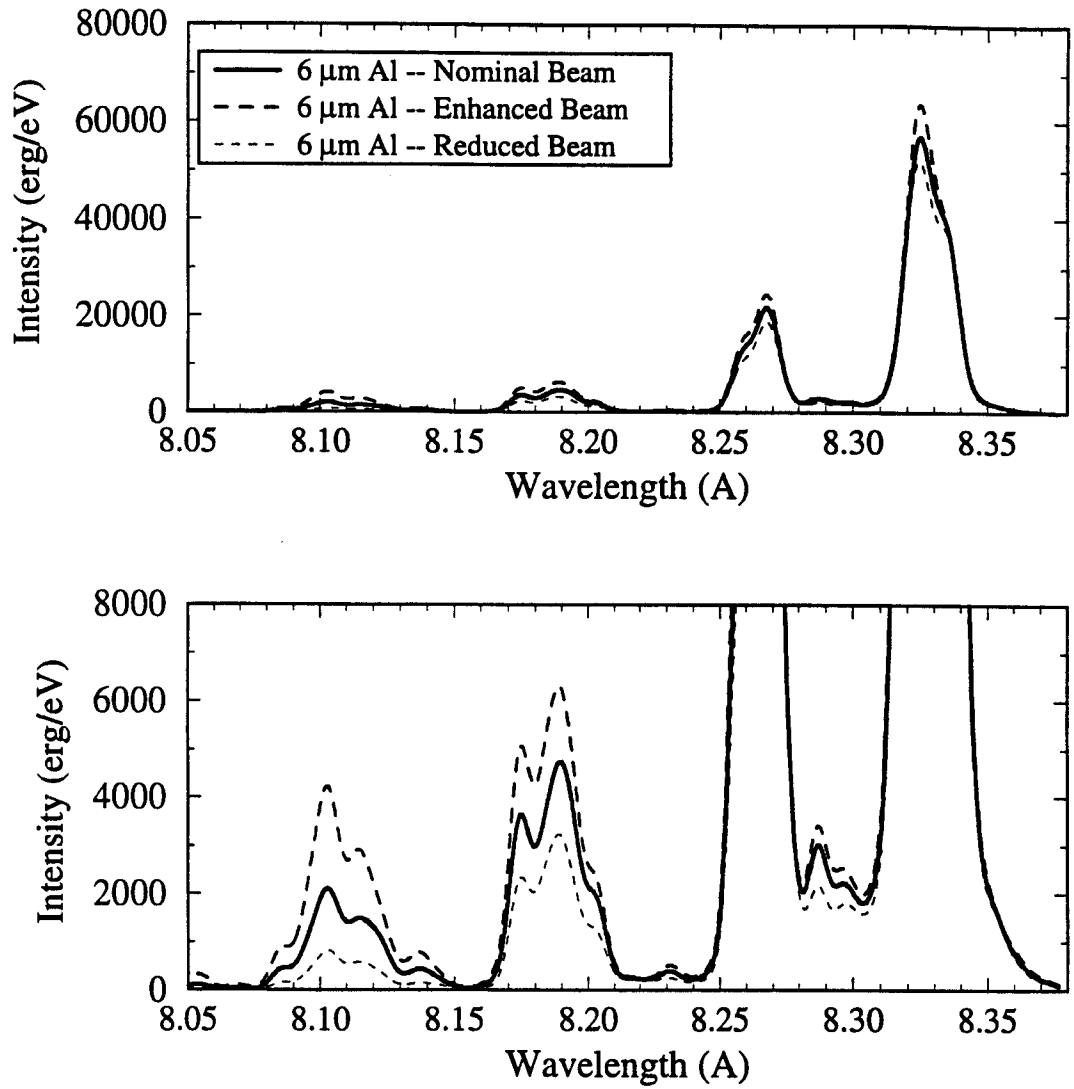


Figure 16. Comparison of space- and time-integrated  $K_{\alpha}$  spectra for 6  $\mu\text{m}$  Al targets using beam current density multipliers of 0.75, 1.0, and 1.25. Bottom plot shows same results on a different scale.

B in Figure 14), a more strongly peaked beam current distribution (vs. Eq. (1)) could produce better agreement with experiment.

Finally, Figure 15 shows a comparison of the 2  $\mu\text{m}$ -thick and 6  $\mu\text{m}$ -thick Al results. The results are very similar, with the emission from the 2  $\mu\text{m}$  case being slightly lower. Experimental results, however, suggest (Figure 1) the emission from a 2  $\mu\text{m}$ -thick target was about a factor of 2 lower than the 6  $\mu\text{m}$  case. The cause of this apparent discrepancy is not understood at this time. Possible explanations include shot-to-shot variations in the proton beam parameters, and absolute calibration of the spectrometer.

The above results represent preliminary calculations performed to provide an understanding of the  $\text{K}_\alpha$  emission spectra obtained in recent KALIF applied-B diode experiments. It is anticipated that additional simulations will be performed later this year.

## **Acknowledgement**

Support for this work has been provided by Forschungszentrum Karlsruhe.

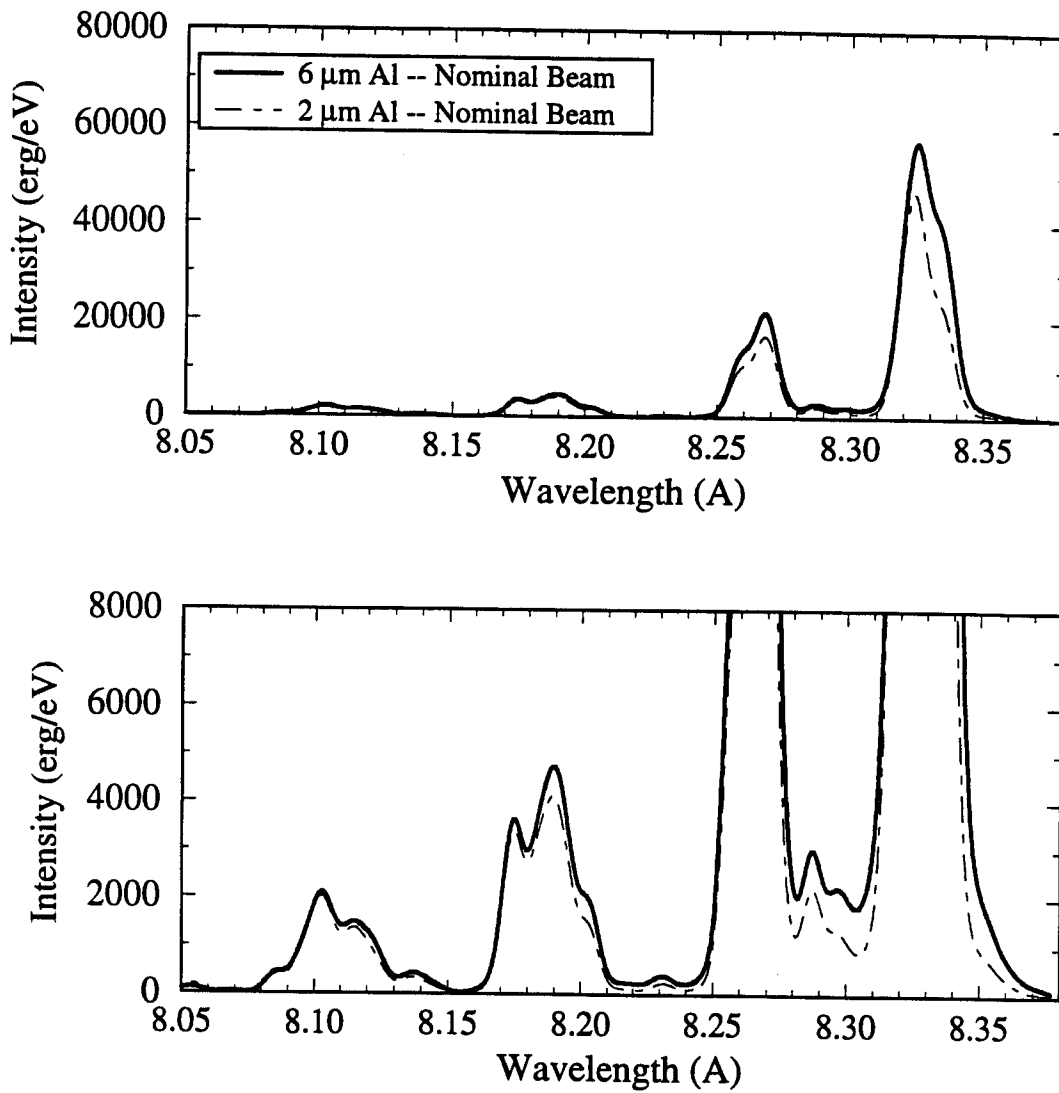


Figure 17. Comparison of space- and time-integrated  $K_{\alpha}$  spectra for 2  $\mu\text{m}$  and 6  $\mu\text{m}$  Al targets. Bottom plot shows same results on a different scale.

## References

1. Meisel, G., et al., “Temperature Measurement for KALIF Targets by Soft X-ray Spectroscopy,” (preliminary version, 1996).
2. Supplied by B. Goel, private communication (Oct. 1995).
3. MacFarlane, J.J., and Wang, P., “Simulation of KALIF Applied-B Diode Shock Wave Physics Experiments,” Fusion Power Associates Report FPA-96-1 (February 1996).
4. MacFarlane, J.J., Moses, G.A., and Peterson, R.R., “BUCKY-1 – A 1-D Radiation-Hydrodynamics Code for Simulating Inertial Confinement Fusion High Energy Density Plasmas,” University of Wisconsin Fusion Technology Institute Report UWFD-984 (August 1995).
5. MacFarlane, J.J., “NLTE – A Code for Computing the Radiative Properties of Non-LTE Plasmas,” Fusion Power Associates Report FPA-93-6 (December 1993).
6. Wang, P., “ATBASE User’s Guide,” Fusion Power Associates Report FPA-93-7 (December 1993).
7. MacFarlane, J.J., and Wang, P., “Numerical Simulation of High Energy Density Plasmas in KALIF Beam-Target Interaction Experiments,” Fusion Power Associates Report FPA-95-3 (December 1995).
8. MacFarlane, J.J., Wang, P., Bailey, J., Mehlhorn, T.A., Dukart, R.J., and Mancini, R.C., *Phys. Rev.* **E47**, 2748 (1993).